Research Article | Vol. 25, No. 12 | 12 Jun 2017 | OPTICS EXPRESS 13714
Optics EXPRESS

Solid-state source of intense yellow light based on a Ce:YAG luminescent concentrator

JUNA SATHIAN,* JONATHAN D. BREEZE, BENJAMIN RICHARDS, NEIL MCN. ALFORD, AND MARK OXBORROW

Department of Materials, Imperial College London, Exhibition Road, London, SW7 2AZ, UK
**j.sathian@imperial.ac.uk*

Abstract: A luminescent concentrator functioning as a bright source of yellow light is reported. It comprises a waveguide made of cerium-doped YAG crystal, in the form of a long-thin rectangular strip, surrounded by flowing air and optically pumped from both sides with blue light from arrays of high-efficiency InGaN LEDs. Phosphor-converted yellow light, generated within the strip, is guided to a glass taper that is butt-coupled to one of the strip's end faces. Up to 20 W of optical power, centered on 575 nm with a linewidth of 76 nm, can be continuously radiated into air from the taper's 1.67 mm × 1.67 mm square output aperture. The intensity of the outputted light is significantly greater than what any yellow (AlGaInP) LED can directly produce (either singly or arrayed), with only a modest increase in linewidth. Furthermore, the wall-plug efficiency of the source exceeds that of any yellow laser. The concept allows for further substantial increases in intensity, total output power and wall-plug efficiency through scaling-up and engineering refinements.

OCIS codes: (230.0230) Optical devices; (230.3670) Light-emitting diodes; (160.5690) Rare-earth-doped materials; (220.1770) Concentrators; (260.3800) Luminescence.

References and links

1. Philips, "MASTER SOX-E PSG 36W BY22d T501SL/12," http://www.lighting.philips.com/main/prof/lamps/high-intensity-discharge-lamps/sox-low-pressure-sodium/master-sox-e-psg/928148200058_EU/product.
2. E. Technologies, "PE300C-10F Cermax Xenon Short Arc Ceramic Body Elliptical Lamp," http://www.excelitas.com/Lists/Cermax%20Lamps/DispForm.ggfgaspx?ID=1.
3. Philips Lumileds Lighting Company, "LXZ1-PL01," http://www.leds.de/out/media/64117_farbige_Luxeon_Z_DS105(1). pdf.
4. M. Enderlein, A. Friedenauer, R. Schwerdt, P. Rehme, D. Wei, V. Karpov, B. Ernstberger, P. Leisching, W. R. Clements, and W. G. Kaenders, "Series production of next-generation guide-star lasers at TOPTICA and MPBC," Proc. SPIE **9148**, 914807 (2014).
5. T. Omi, S. Kawana, S. Sato, and M. Honda, "Ultrastructural changes elicited by a non-ablative wrinkle reduction laser," Lasers Surg. Med. **32**(1), 46–49 (2003).
6. B. C. Rowan, L. R. Wilson, and B. S. Richards, "Advanced Material Concepts for Luminescent Solar Concentrators," IEEE J. Sel. Top. Quantum Electron. **14**(5), 1312–1322 (2008).
7. W. G. J. H. M. van Sark, "Luminescent solar concentrators – A low cost photovoltaics alternative," Renew. Energy **49**, 207–210 (2013).
8. Y. Yang, I. D. W. Samuel, and G. A. Turnbull, "The development of luminescent concentrators for pumping organic semiconductor lasers," Adv. Mater. **21**(31), 3205–3209 (2009).
9. A. Barbet, A. Paul, T. Gallinelli, F. Balembois, J. P. Blanchot, S. Forget, S. Chénais, F. Druon, and P. Georges, "Light-emitting diode pumped luminescent concentrators: a new opportunity for low-cost solid-state lasers," Optica **3**(5), 465–468 (2016).
10. G. S. Atoyan, V. A. Gladyshev, S. N. Gninenko, V. V. Isakov, A. V. Kovzelev, E. A. Monich, A. A. Poblaguev, A. L. Proskuryakov, I. N. Semenyuk, V. G. Lapshin, Y. V. Protopopov, V. I. Rykalin, and V. K. Semenov, "Lead-scintillator electromagnetic calorimeter with wavelength shifting fiber readout," Nucl. Instrum. Methods Phys. Res. A **320**(1-2), 144–154 (1992).
11. G. Colantuono, A. Buckley, and R. Erdelyi, "Ray-Optics Modelling of Rectangular and Cylindrical 2-Layer Solar Concentrators," J. Lightwave Technol. **31**(7), 1033–1044 (2013).
12. L. R. Wilson, "Luminescent solar concentrators: a study of optical properties, re-absorption and device optimisation," Thesis, Heriot-Watt University (2010).

#287744 https://doi.org/10.1364/OE.25.013714
Journal © 2017 Received 1 Mar 2017; revised 21 Apr 2017; accepted 22 Apr 2017; published 8 Jun 2017

Optics EXPRESS

13. V. Bachmann, C. Ronda, and A. Meijerink, "Temperature quenching of yellow Ce^{3+} luminescence in YAG:Ce," Chem. Mater. **21**(10), 2077–2084 (2009).
14. X. Yang, H. Li, Q. Bi, L. Su, and J. Xu, "Growth of large-sized Ce:$Y_3Al_5O_{12}$ (Ce:YAG) scintillation crystal by the temperature gradient technique (TGT)," J. Cryst. Growth **311**(14), 3692–3696 (2009).
15. S. Murai, M. A. Verschuuren, G. Lozano, G. Pirruccio, A. F. Koenderink, and J. G. Rivas, "Enhanced absorption and emission of $Y_3Al_5O_{12}$: Ce^{3+} thin layers prepared by epoxide-catalyzed sol-gel method," Opt. Mater. Express **2**(8), 1111–1120 (2012).
16. S. M. Kaczmarek, G. Domianiak-Dzik, W. Ryba-Romanowski, J. Kisielewski, and J. Wojtkowska, "Changes in Optical Properties of Ce:YAG Crystals under Annealing and Irradiation Processing," Cryst. Res. Technol. **34**(8), 1031–1036 (1999).
17. A. Goetzberger and V. Wittwer, "Fluorescent planar collector-concentrators: a review," Sol. Cells **4**(1), 3–23 (1981).
18. M. Khoshakhlagh, J. P. Islamian, S. M. Abedi, and B. Mahmoudian, "Development of scintillators in nuclear medicine," World J. Nucl. Med. **14**(3), 156–159 (2015).
19. C. Varney, D. Mackay, S. Reda, and F. Selim, "On the optical properties of undoped and rare-earth-doped yttrium aluminium garnet single crystals," J. Phys. D Appl. Phys. **45**(1), 015103 (2012).
20. J. Mares, B. Jacquier, C. Pedrini, and G. Boulon, "Energy transfer mechanisms between Ce^{3+} and Nd^{3+} in YAG:Nd, Ce at low temperature," Rev. Phys. Appl. (Paris) **22**(2), 145–152 (1987).
21. S. Arjoca, E. G. Víllora, D. Inomata, K. Aoki, Y. Sugahara, and K. Shimamura, "Temperature dependence of Ce:YAG single-crystal phosphors for high-brightness white LEDs/LDs," Mater. Res. Express **2**(5), 055503 (2015).
22. Y. Kawamura, H. Sasabe, and C. Adachi, "Simple accurate system for measuring absolute photoluminescence quantum efficiency in organic solid-state thin films," Jpn. J. Appl. Phys. **43**, 7729–7730 (2004).
23. L.-O. Pålsson and A. P. Monkman, "Measurements of solid-state photoluminescence quantum yields of films using a fluorimeter," Adv. Mater. **14**(10), 757 (2002).
24. C. L. Mulder, P. D. Reusswig, A. M. Velázquez, H. Kim, C. Rotschild, and M. Baldo, "Dye alignment in luminescent solar concentrators: I. Vertical alignment for improved waveguide coupling," Opt. Express **18**, A79–A90 (2010).
25. T.-S. Ahn, R. O. Al-Kaysi, A. M. Müller, K. M. Wentz, and C. J. Bardeen, "Self-absorption correction for solid-state photoluminescence quantum yields obtained from integrating sphere measurements," Rev. Sci. Instrum. **78**(8), 086105 (2007).
26. L. R. Wilson, B. C. Rowan, N. Robertson, O. Moudam, A. C. Jones, and B. S. Richards, "Characterization and reduction of reabsorption losses in luminescent solar concentrators," Appl. Opt. **49**(9), 1651–1661 (2010).
27. T. Smith and J. Guild, "The CIE colorimetric standards and their use," Trans. Opt. Soc. **33**(3), 73–134 (1931).
28. M.R Wernand and H. J. Van der Woerd, "Spectral analysis of the Forel-Ule Ocean colour comparator scale," J. Eur. Opt. Soc, Rapid Publ. **5**, 10014 (2010).
29. W. Shurcliff and R. C. Jones, "The trapping of fluorescent light produced within objects of high geometrical symmetry," J. Opt. Soc. Am. A **39**(11), 912–916 (1949).
30. S. Roelandt, Y. Meuret, D. K. de Boer, D. Bruls, P. Van De Voorde, and H. Thienpont, "Incoupling and outcoupling of light from a luminescent rod using a compound parabolic concentrator," Opt. Eng. **54**(5), 055101 (2015).
31. J. Sansregret, J. M. Drake, W. R. Thomas, and M. L. Lesiecki, "Light transport in planar luminescent solar concentrators: the role of DCM self-absorption," Appl. Opt. **22**(4), 573–577 (1983).
32. J. L. Banal, J. M. White, K. P. Ghiggino, and W. W. Wong, "Concentrating aggregation-induced fluorescence in planar waveguides: a proof-of-principle," Sci. Rep. **4**(1), 4635 (2014).
33. P. P. Verbunt and M. G. Debije, " Progress in luminescent solar concentrator research: solar energy for the built environment," *in World Renewable Energy Congress* (2011), pp. 2751–2758.
34. J. Breeze, K.-J. Tan, B. Richards, J. Sathian, M. Oxborrow, and N. M. Alford, "Enhanced magnetic Purcell effect in room-temperature masers," Nat. Commun. **6**, 6215 (2015).

1. Introduction

The spectral sensitivity of the cone opsins in a human retina and the spectral absorptance of hemoglobin in human blood mean that significant consumer applications, such as full-color video projection and vascular skin surgery, require intense sources of yellow light. In these applications, the light needs to be supplied either continuously, i.e., CW, or in pulses hundreds of microseconds in duration. On the scales set by current laser technology, this quasi-continuous light need only be of modest instantaneous power, intensity, and monochromaticity (inverse linewidth). For reasons of practicality and economy, it should also be generated at high wall-plug efficiency (WPE). To date, all of the established types of light source, including lasers, struggle to provide it: LEDs lack intensity, yellow lasers lack efficiency, and lamps lack either one or the other. Beyond what is technically possible and even if the source's energy and maintenance costs are deemed tolerable, safety hazards and

Optics EXPRESS

the further costs and inconveniences of their associated control measures, often impact severely on the relevant application's overall viability.

Rhodamine-based long-pulse dye lasers are used successfully for vascular skin surgery and cosmetic treatments, but the toxic and, in most systems, highly flammable nature of the gain medium, which deteriorates with usage, is troublesome in a clinical or consumer setting. The high operating temperatures and thus long warm-up times of copper-vapour lasers and the explosion hazard and limited lifetime of high-pressure xenon arc lamps make neither consumer-friendly technologies. Table 1 quantifies the technical state of the yellow-light source art; given the scientific scope of this paper, we have not attempted to cost out the maintenance and safety issues.

Table 1. The relative performances/attributes of different types of yellow light sources

	Unit	Low-pressure sodium vapour lamp	Short arc xenon lamp - spectrally filtered*	High-efficiency AlGaInP LED	Diode-pumped solid state laser	Long-pulsed medical dye laser (rhodamine)	InGaN-pumped Ce:YAG luminescent concentrator
Exemplar		Philips SOX-E PSG 36 W	Excelitas PE300C-10F (300 W)	Philips Lumiled LXZ1-PL01	Toptica Sodium Star	Chromo-genex Nlite-V	This work
Linewidth	nm	0.6	*50 assumed	15	$<10^{-5}$	<1	76
Output power[(a)]	W	11 -all directions	2.2 (through a 6 mm dia. aperture)	0.12	20	2×10^{3} [(b)]	20
Wall-plug efficiency (WPE)	%	30	0.7	11	2	1	2
Output intensity	W/mm^2	few $\times 10^{-4}$	few $\times 10^{-2}$	~0.1	$\sim 10^{7}$	few $\times 10^{5}$	7.2
Cost [(c)]	USD	$\sim 10^{2}$	$\sim 10^{2}$	few	$\sim 10^{5}$	few $\times 10^{4}$	few $\times 10^{3}$
References		[1]	[2]	[3]	[4]	[5]	

(a) Instantaneous power during a pulse 500 μs in duration ("quasi-continuous" operation); the time-averaged power.

(b) Instantaneous power during pulse.

(c) Purchase cost per single device (at high volumes); additional costs associated with operation/maintenance/liability/disposal not included.

Luminescence concentration, also known as fluorescence concentration when the emitter is a fluorophore, provides an alternative mechanism to stimulated emission for converting pump light from a primary source into secondary light of greater intensity —though of longer wavelength. Almost all of the research done on luminescent/fluorescent concentrators to date [6,7] has focused on their use as harvesters of solar photons, outputting light into photovoltaic cells. Occasionally, luminescent concentrators (LCs) have been used to pump lasers [8,9]. They also perform as wavelength shifters, often in the form of fibers for channeling light towards photomultipliers and in nuclear (gamma-ray) scintillation detectors [10]. Here we consider LCs as secondary sources of light in their own right, serving applications directly.

The present work describes the design, construction, characterization and modelling of an LC light source based on a strip of cerium-doped YAG, whose measured performance is stated in the right-hand column of Table 1.

Optics EXPRESS

2. Design and construction

2.1 Design fundamentals

Previous studies have modelled luminescent concentrators in the form of flat rectangular plates [7,11]. This geometry covers the long-thin rectangular strips considered here, where the plate's length-to-width and width-to-thickness aspect ratios are both high. Let the length, width and thickness of our plate be, l, w, t respectively. For simplicity, we assume that the LC is pumped uniformly across its two largest ($l \times w$) surfaces. The optical processes within a luminescent concentrator are identified in Fig. 1.

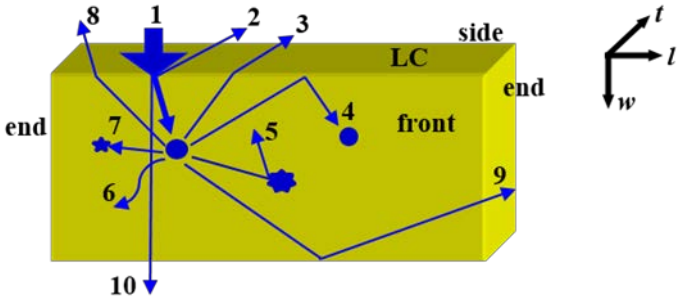

Fig. 1. Cross section of generic luminescent concentrator. Here, the incident pump light (1) is absorbed by a luminophore (blue circle) whereupon it is re-emitted at a different (longer) wavelength, at a given quantum efficiency. Some of this light (9) reaches the light output end by total internal reflection (TIR). Loss mechanisms include surface reflection (2), escape (3), self-absorption (4), inclusion scattering (5), non-radiative decay (6), host absorption (7), surface scattering (8) and no photon absorption (10).

The power outputted by an LC is given by $P_{\text{pump}}^{\text{opt}}\eta_{\text{opt}}$, where $P_{\text{pump}}^{\text{opt}}$ in the inputted optical pump power and η_{opt} is the LC's optical conversion efficiency. For a rectangular LC, the intensity of its outputted light is $\left(P_{\text{pump}}^{\text{opt}} \times \eta_{\text{opt}}\right)/(w \times t)$. The conversion efficiency can be expressed as a product of factors associated with the different loss mechanisms [7,12] depicted in Fig. 1.

$$\eta_{\text{opt}} = (1-R)\eta_{\text{abs}}\eta_{\text{PLQY}}\eta_{\text{Stokes}}\eta_{\text{TIR}}\eta_{\text{trap}}\eta_{\text{host}}\eta_{\text{SA}} \quad (1)$$

where the order is from left to right. Here, $(1-R)$ is the loss due to Fresnel reflection upon the pump light entry into the LC, η_{abs} represents the efficiency at which the incoming photons are absorbed, η_{PLQY} is the photoluminescence quantum yield, which is the number of photons emitted for each photon absorbed, η_{Stokes} is the Stokes efficiency and accounts for the energy loss due to Stokes shift, η_{TIR} is the TIR efficiency, η_{trap} is the light trapping efficiency and equals the probability that the direction of an emitted photon is such that the photon undergoes TIR —as opposed the direction lying within an escape cone, so allowing the photon to escape the LC, η_{host} takes into account losses within the host due to both absorption and scattering, and η_{SA} is the fraction of photons reaching the light collection end of the LC without undergoing self-absorption.

2.2 Materials science: Why Ce:YAG?

It is known [13–15] that cerium-doped YAG, upon absorbing blue light, emits yellow light in the 500–700 nm wavelength range, peaking at 536 nm (at room temperature and without self-

Optics EXPRESS

absorption, i.e., in the low-concentration limit). This luminescence corresponds to transitions from the Ce^{3+} ion's lowest 5d level to its two 4f levels. However, excited state absorption precludes its use as a (yellow) laser gain medium [16]. It is commonly used as a light-converting phosphor in InGaN-based white-light-emitting diodes [17]. Ce:YAG crystals are also used in medical imaging [18] and as radiation scintillators [14]. The near complete separation between its absorption and emission spectrum, together with its high quantum yield, short emission lifetime, high thermal conductivity and thermal stability, makes Ce:YAG advantageous for use as a luminescent concentrator [14,15,19]. Ce:YAG's luminescent yield suffers no significant thermal quenching provided the concentration of its dissolved Ce^{3+} ions lies below 1% and the temperature remains below 600 K; it can thus sustain luminescence concentration even under intense optical pumping with associated high heat loading [13]. Self-absorption also increases with temperature as spectral overlap increases, which can lead to a decrease in efficiency. In this experiment the temperature of the Ce:YAG crystal was kept well below 400 K by forced air cooling. The other process that can have an adverse effect on the absorption and luminescence properties of the Ce:YAG crystal is the growth atmosphere where it is reported that the presence of hydrogen enhances the luminescence [19].

2.3 Thermal design

The blue-to-yellow Stokes shift associated with Ce:YAG's photoluminescence, in conjunction with its less-than-perfect quantum yield [Sections 3.2 and 4.1.1 estimate its Photoluminescence quantum yield (PLQY) to be 88%] means that at least a quarter of the optical pump energy absorbed by a luminescent concentrator made of Ce:YAG is converted to heat. This heat can be removed more effectively if the LC is thin with a high surface area, where all emitters inside the crystal lie a short distance from the surface, over which coolant can flow. In the devices reported here, forced air blown by an electric-powered fan served both as a coolant and as the optical waveguide's cladding.

2.4 *Practical realization*

The shape and dimensions of the LC were severely constrained by the Ce:YAG material available to us. This originated from an irregularly-shaped remnant, from which several cylindrical rods (not in our possession) had long-since been cored and removed. The remnant had composed a wedge cut from a much larger boule of monocrystalline Ce:YAG, grown at Union Carbide Corp.'s Crystal Products Division, in Washougal, WA, USA. Our sample's longest dimension was approx. 80 mm. It was first sawn into a number of prismatic bars. These were subsequently banked together and planed (using a surface grinder) to yield a number of nominally identical rectangular bars, each approx. 77 mm × 8.5 mm × 4.5 mm in dimension; these operations, were done with diamond tools, at National Physical Laboratory (NPL), Teddington, UK. The chemical composition of the sample was verified using a LEO Gemini 1525 FEGSEM coupled with an energy dispersive spectrometer (EDS). The material's optical absorption depth (inverse of its Beer-Lambert absorption coefficient) at the LC's pump wavelength (460 nm), and thus the substitutional concentration of the cerium dissolved within the Ce:YAG was measured using an Agilent Cary 5000 UV-Vis-NIR Spectrophotometer. The UV-Vis absorption spectrum of the sample is shown in Fig. 2. Measurements were performed on a 0.34 mm Ce:YAG sample in the form of an irregularly-shaped thin plate. The Beer-Lambert law and the known absorption cross-section of cerium in YAG (3×10^{-18} cm^2) [20,21] were used to calculate the optical absorption depth 100 µm and the concentration of cerium 0.11% in substitution to yittrium. The material's optical qualities were excellent: no observable inclusions, strain or twinning when viewed through crossed-polarizers.

Optics EXPRESS

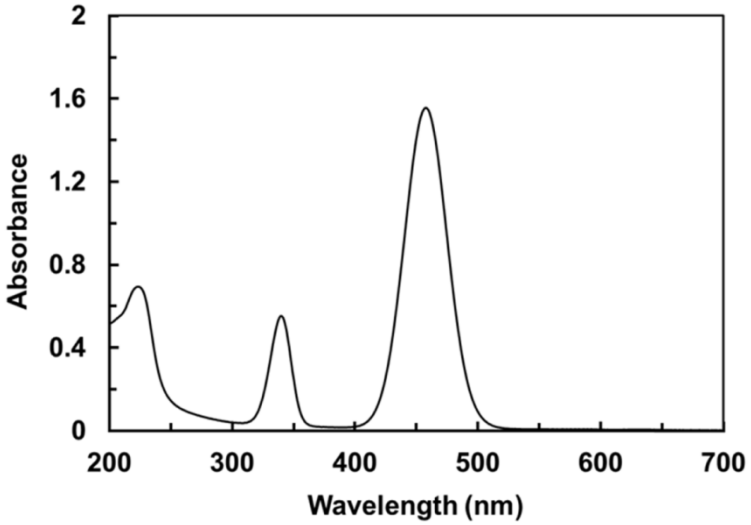

Fig. 2. UV-Vis absorbance measurement of Ce:YAG crystal.

With the above optical depth in mind, one of the Ce:YAG bars was cut and diced lengthways (77 mm long by 4.5 mm deep), using a thin-blade wafer-saw into strips approximately 0.6 mm thick. The main plane-parallel faces of these strips were then lapped and polished. These slicing and polishing operations were done at SurfaceNet GmbH, Rheine, Germany. The strip's remaining side and end faces were then lapped and polished at IC Optical Systems (ICOS) Ltd, Beckenham, UK, resulting in a set of nominally identical rectangular strips, with dimensions 76 mm × 4.26 mm × 0.57 mm. Though their thickness (0.57 mm) was many times greater than the material's above-stated optical absorption depth (so reducing the LC's geometric gain), thinner strips could not have been cut and handled (at least not without fear of breakages) given the equipment/resources available.

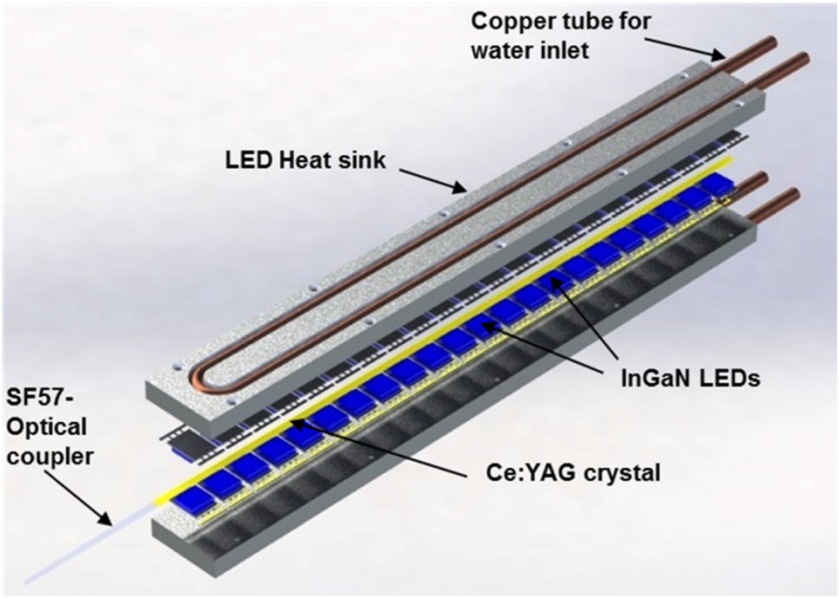

Fig. 3. Ce:YAG luminescent concentrator light source.

Optics EXPRESS

Uncalibrated transmission measurements were performed on the plane-parallel-polished pieces of Ce:YAG. These used a 445 nm Nichia NDB7875 laser diode fed by a current-stabilized power supply, a Photon Control (Melles Griot) optical power meter and a dichroic mirror to reject the yellow luminescence. Each piece could be moved into the laser beam to probe different regions of its interior, and different pieces of the same optical thickness were swapped into and out of the beam. No noticeable change in the absorption for pieces of the same thickness, could be observed within the few-percent precision imposed by the instability in the laser diode's output power and the variable quality of the optical polish of surfaces (as could be judged qualitatively by the amount scatter). The concentration of Ce^{3+} in the Ce:YAG sample was thereupon presumed to be uniform. The final embodiment of our LC (Fig. 3) comprised four such Ce:YAG strips, butt-coupled in series through 0.57 mm × 4.26 mm rectangular joints, made using refractive-index-matched optical glue containing nanoparticles (Pixelligent Technologies LLC, MD, USA).

One end of the jointed-together strip (now 4 × 76 = 304 mm long) was optically butt-coupled to the large end of a taper (Schott SF57 glass) whose refractive index (1.846) lies close to that of Ce:YAG (1.83) at yellow wavelengths. At its other end, the taper was square in cross section with a 1.67 mm side length. The same Pixelligent Technologies high-R.I glue was also used to make the Ce:YAG-to-SF57 optical joint (still 0.57 mm × 4.26 mm rectangular). This taper was bespoke made by ICOS Ltd. The LC waveguide was then sandwiched between two banks of InGaN pump LEDs, with its two 304 mm × 4.26 mm input faces towards opposing LED banks. Each bank was made from prefabricated 50 W (input power) modules, each containing a wire-bonded array of closely-packed LED dies fixed to a common insulated aluminum substrate. Spectrally, the output of these LEDs peaked at 460 nm, red-shifting by a few nm at high applied current/power (die temperature). The substrates of the modules were first trimmed to reduce the dead space between adjoining LED arrays, then arranged and glued in a row on the cold-face of water-cooled aluminum-copper heat sink (supplied by PSL Assemblies Ltd., England, UK), using thermally-conductive epoxy (EPO-TEK H70E). Slotted between the LED arrays secured by the same glue, were a series of identical knife-edge supports cut from thin stainless steel sheet. Each support had one horizontal knife edge, which mechanically supported the LC strip a mm or so vertically above the lower LED bank, and two opposing vertical knife edges, which constrained the jointed Ce:YAG strip to lie collinearly and centrally with respect to same. Bolts and spacers joining the top and lower banks mechanically together ensured that it too lay collinearly with an equal air gap above and below the LC strip through which forced cooling air could flow at high speed.

3. Experimental technique

Our experiments were conducted on four different pieces of Ce:YAG;

(a) a thin plate (irregular shape): 13.26 mm × 0.34 mm

(b) a single strip: 76 mm × 4.26 mm × 0.57 mm

(c) a short strip: 22 mm × 4.26 mm × 0.57 mm

(d) 4-in-a-row (butt-jointed together with glue) long composite strip of dimensions 304 mm × 4.26 mm × 0.57 mm. Only the main plane-parallel surfaces of (a) were polished. All surfaces of (b)-(d) were polished.

3.1 Output spectrum and total outputted power

A spectrum of the source, averaged over all directions, was measured by inserting the LC's output aperture into the entry port of a home-made integrating sphere. The receiving aperture of an Ocean Optics USB2000 + Fiber Optic Spectrometer was inserted into its exit port [same arrangement as in Fig. 4]. Our sphere was 20 cm in diameter and everywhere coated

Optics EXPRESS

(internally) with barium sulphate-loaded paint (Pro-Lite Technology Ltd., England, UK). The sphere included a baffle (also coated white) that mutually obscured the sphere's entry and exit ports. These ports were both 8 mm in diameter. Without removing it from the integrating sphere, the same source's total angle-averaged optical output power could be determined by replacing the fiber-coupled spectrometer from the sphere's output port with a silicon detector (Vishay BPW21R) of known spectral response. With the source removed, the absolute sensitivity of the integrating sphere with this detector was determined at spot wavelengths (445 nm, 532 nm, 589 nm and 632 nm) by injecting laser beams of known absolute power (measured using a calibrated Photon Control [Melles Griot] optical power meter) into the sphere's input port.

3.2 Photoluminescence quantum yield (PLQY)

The experimental set-up shown in Fig. 4(a) was used. The 0.34 mm thin plate Ce:YAG sample was placed inside the integrating sphere. Its luminescence was measured using the same Ocean Optics USB2000 + spectrometer attached to the sphere's exit port as before. This sample was struck by a 1 mW beam from the same Nichia NDB7875 445 nm laser diode (attenuated using neutral density filters). Self-absorption losses could be ignored on account of the sample's thinness. The determination of the sample's PLQY exactly followed an established method described in the literature [22,23].

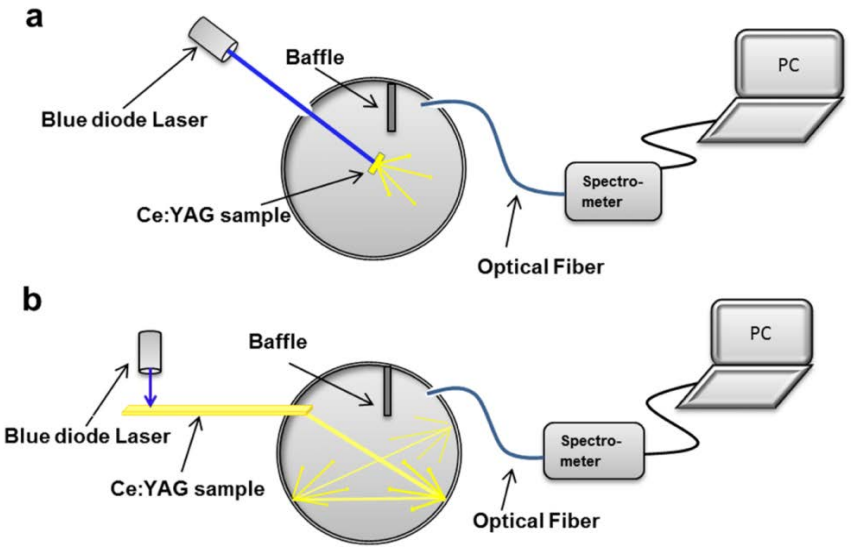

Fig. 4. The schematic of the experimental set-up used to measure the (a) Photoluminescence quantum yield (PLQY), Trapping efficiency, η_{trap} and (b) self-absorption efficiency, η_{SA} of the Ce:YAG sample.

3.3 Stokes shift

The Stokes shift was determined using the experimental set-up as PLQY [Fig. 4(a)] and is given by the energy difference between the absorption and emission peaks. The ratio of these energies gives the Stokes efficiency.

3.4 Trapping efficiency

The trapping efficiency η_{trap} of the emitted photons inside the Ce:YAG strip was measured using the set-up in Fig. 4(a). The emission collected with all sides and end faces (Fig. 1)

Optics EXPRESS

blackened was compared against the full emission profile of the 22 mm sample. The trapping efficiency was calculated using the equation [24]:

$$\eta_{\text{trap}} = \frac{\int [F_{\text{em}}(\lambda) - F_{\text{face}}(\lambda)]\, d\lambda}{\int F_{\text{em}}(\lambda)\, d\lambda} \tag{2}$$

Here $F_{\text{em}}(\lambda)$ is the luminance from the whole sample and $F_{\text{face}}(\lambda)$ is the emission when all LC's sides and end faces are blackened.

3.5 Self-absorption efficiency

We define the self-absorption efficiency, η_{SA}, [determined using the experimental set-up in Fig. 4(b)] as the probability that the generated fluorescent photon will reach the detector without undergoing self-absorption [25,26]:

$$\eta_{SA} = 1 - \frac{\int F_2(\lambda)\, d\lambda}{\int F_1'(\lambda)\, d\lambda} \tag{3}$$

where $F_1(\lambda)$ is Ce:YAG's emission spectrum (in units of watts per nm) in the low-concentration or thin-sample limit, for which self-absorption effects (including power loss and spectral red-shifting) vanish, $F_1'(\lambda)$ is the scaled luminance spectrum measured for the 76 mm single strip and $F_2(\lambda)$ is the observed (unscaled) luminance spectrum for the 76 mm strip. $F_1'(\lambda)$ is obtained by scaling $F_1(\lambda)$ to match $F_2(\lambda)$ at wavelengths above 680 nm where self-absorption is minimal. Alternatively, η_{SA} can also be calculated from the energy difference between the two emission spectra, $F_1(\lambda)$ and $F_2(\lambda)$.

4. Results and determination of key design parameters

On excitation from banks of blue InGaN LEDs, a single strip (76 mm long) of the Ce:YAG outputted yellow light from its end face. This light's spectrum is displayed in Fig. 5(a), with a peak emission at 548 nm, only slightly red-shifted from Ce:YAG's intrinsic room-temperature emission profile (no self-absorption) at low concentration [13–15].

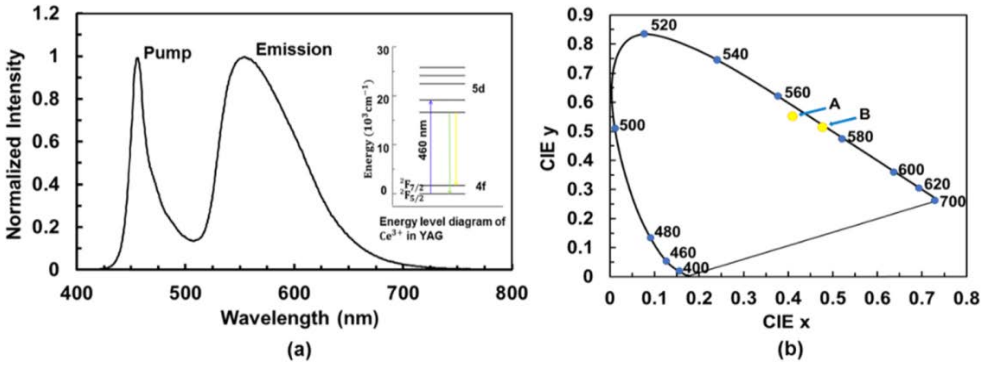

Fig. 5. (a) Output spectrum of LC light source —76 mm long (here the pump spectrum is included at 460 nm) and (b) the CIE (1931) colour space chromaticity diagram; CIE coordinates (yellow dots) A (0.416, 0.565) with 0.95 calculated emission saturation (purity) for the 76 mm LC light source, and B (0.481, 0.510) and 0.985, respectively, for the four-strip LC light source.

Optics EXPRESS

Figure 5(b) shows the 1931 CIE chromaticity diagram and the chromaticity coordinates for the two light sources; A (0.416, 0.565) for the 76 mm-single strip LC and B (0.481, 0.510) for the four-strip LC light source [27,28]. The dominant wavelengths of the LCs emitted light are at 565 nm and 575 nm, respectively, and these correspond to the center wavelength of their emission spectra. The emission colour saturation or purity of the two LCs light output are 0.95 and 0.985, respectively.

The total power emitted from one end of a single Ce:YAG strip, as a function of the electrical power inputted into its associated pump diodes is displayed in Fig. 6; for the results shown here no taper was attached. The power is plotted both in the case of the strip's other end being naked (just like the outputting end) and in the case of it being covered by (and optically coupled to) a solid aluminum mirror reflecting light back into the strip. In the latter case, the total optical output power exceeded 7 W at 160 W of input electrical power. The WPE, fitting a straight line (through the origin) to the data shown, provides an already impressive value of 5.08 ± 0.30%.

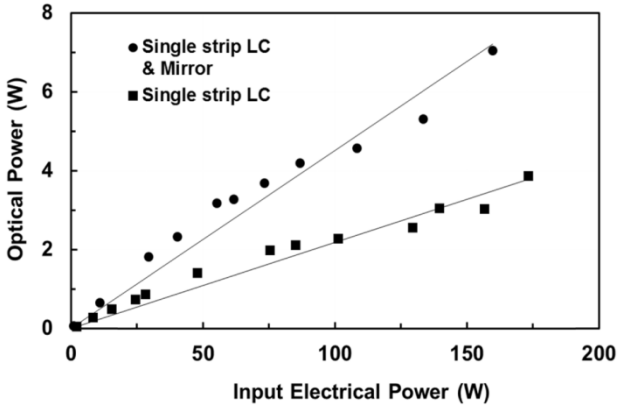

Fig. 6. The optical output power for a single strip LC.

The output power as a function of the input power for the four-strips-in-series arrangement (with a mirror at its non-outputting end and a glass taper at the light outputting end) is shown in Fig. 7.

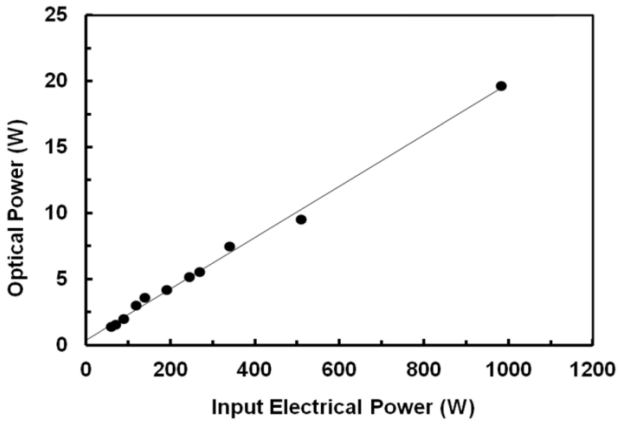

Fig. 7. The optical output power for a four-strip LC.

The maximum optical output power obtained is 20 W, still maintaining a WPE > 2.0%, which corresponds to an output intensity of 7.2 W/mm^2 (Fig. 7). The decrease in WPE can be attributed to self-absorption, losses at the joints and light outcoupling losses at the detector. A

Optics EXPRESS

mirror at the back end of the fourth Ce:YAG strip increased the output to an additional 15% only, due to these losses.

4.1 Optical conversion efficiency

The WPE of the LC device gives an insight into the optical efficiency of the system, but for a complete understanding of the process, the optical efficiency measurement of the Ce:YAG was conducted by separately measuring the individual parameters in Eq. (1). The measurement reported here refer to a single 76 mm × 4.26 mm × 0.57 mm Ce:YAG strip with no output taper unless stated otherwise.

Table 2. Estimates of the parameters affecting the luminescent concentrator's conversion efficiency

parameter	estimate	notes/assumptions
$(1-R)$	0.914	Pump light impinges at normal incidence, for which the reflection loss at the entry surface is $R=[(n-1)/(n+1)]^2$, where the refractive index of Ce:YAG is n = 1.83 (at all relevant wavelengths).
η_{abs}	1.0	No pump light is otherwise scattered or absorbed at the entry surface and the strip is optically thick/opaque —so absorbing the entire pump light that enters it.
η_{PLQY}	0.88	Section 4.1.1
η_{Stokes}	0.812	From the ratio of λ_{max} of the absorption (pump) and emission spectra —Fig. 5(a).
η_{trap}	0.65	Section 4.1.2, considering the fact that there are no side mirrors.
η_{host} , η_{TIR}	1.0	The host imperfections and the TIR losses are assumed to be small.
η_{SA}	0.915	Section 4.1.3
η_{opt}	0.388	

4.1.1 Determining η_{PLQY}

Using the thin plate of Ce:YAG (0.34 mm thick, so as to render self-absorption losses negligible), the PLQY was measured to be 88 ± 3% with the luminescence's emission peak at 536 nm, close to the molecular emission spectrum of Ce:YAG [13,15].

4.1.2 Determining η_{trap}

For a single 76 mm × 4.26 mm × 0.57 mm Ce:YAG strip, using the experimental set-up shown in Fig. 4(a), the trapping efficiency, η_{trap}, was measured to be 81%. This is slightly lower than the theoretical value of $\sqrt{\left(1-1/n_{YAG}^2\right)}$ = 83.7%. Out of these trapped photons the percentage of waveguided photons reaching the edges by TIR depend on the losses owing to repeated self-absorption and re-emission inside the Ce:YAG sample. The converse probability $\left(1-\eta_{trap}\right)$ gives the probability of the escape cone losses, which in our case is 19%. An ideal luminescent concentrator has mirrors on both of its long side faces $(l\times t)$ and one of its short end faces $(w\times t)$ and if excited from the front face $(l\times w)$, the losses from front and back escape cones are only considered. In the current design of the LC, due to the ease of fabrication, we have added only one mirror at the far end, opposite to the light

Optics EXPRESS

collection end, and hence the actual theoretical value for four escape cone losses instead of two will be 32.6% [15,29], the experimental value being 35%. This is included in the optical efficiency calculation in Table 2.

4.1.3 Determining η_{SA}

An assessment of the magnitude of self-absorption effects of the single long Ce:YAG sample was made along the lines of refs [25,26]. Here, the self-absorption-free emission spectrum of our thin-plate Ce:YAG sample is scaled to match the observed luminance at longer wavelengths.

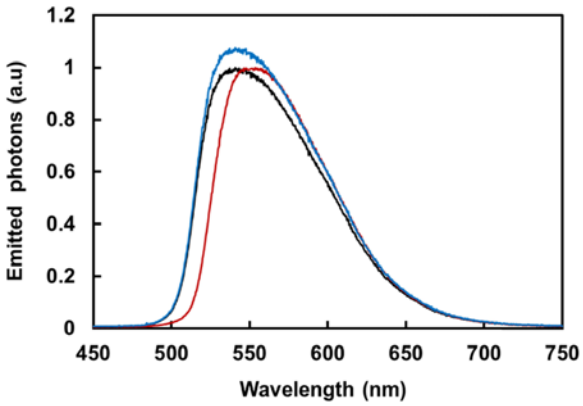

Fig. 8. Normalized true luminescence spectrum (black), $F_1(\lambda)$, the normalized observed luminescence spectrum (red), $F_2(\lambda)$, and the scaled spectrum (blue), $F_1'(\lambda)$ where $F_1'(\lambda)$ matches with observed spectrum $F_2(\lambda)$ at wavelengths above 680 nm.

The self-absorption is depicted here (Fig. 8) as a shift in the emission spectrum due to the absorption of the emitted light within the material over a long path length along with a reduction in the emission intensity. From the calculation (Section 3.5), it is confirmed that the photons emitted from a 76 mm Ce:YAG have 91.5% chance of reaching the detector with the remaining 8.5% of the photons being self-absorbed. The pronounced effect of self-absorption with excitation-point distance for the four-strip LC is conducted using the experimental set-up in Fig. 4(b) and is shown in Fig. 9.

Optics EXPRESS

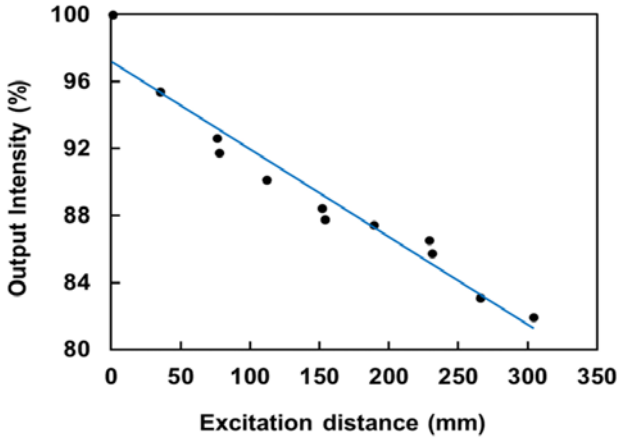

Fig. 9. The decrease in output intensity with excitation-point distance due to self-absorption for a four-strip LC (four-strip Ce:YAG dimensions: 304 mm × 4.26 mm × 0.57 mm). The closely spaced (in excitation distance) values correspond to those on either side of the three optical joints, respectively, and the other values are taken at an interval of 35 mm.

Based on the values appearing in Table 2, the optical efficiency [Eq. (1)] of a single Ce:YAG 76 mm-long strip, with total light outputted from one end (with no reflecting mirror attached) is predicted to be 19.4% (half of the 38.8% in Table 2). But, for the single LC device, the experimental optical efficiency measured using an integrating sphere is ~9.75% (~17% with an end mirror). This can be understood by the fact that the integrating sphere detector collects the light emitted into the air and not the whole trapped light that is available and the 17% optical efficiency is basically the escape cones collectively from the two ends. This was analyzed by butt-coupling the single LC strip's outputting end to a Photon Control (Melles Griot) optical power meter (which uses a flat glass window), using index matching liquid, which gave an optical efficiency ~19% (with no end mirror) close to the calculated value (19.4%) from Table 2. In order to extract all the trapped light, a separate coupler (SF57 glass taper) is designed and is then optically attached to the LC [29,30]. But with an optical coupler added to the end of the LC (with a mirror at the non-outputting end) the experimental output is still ~14.7% indicating losses in our tapered light guide. However the optical coupler concentrates the light into a much smaller spot.

To further investigate the problem, Monte-Carlo ray-tracing simulation of the single 76 mm × 4.26 mm × 0.57 mm Ce:YAG strip was performed. Ray-tracing simulations have been previously successful in understanding the optical efficiency as well as the loss mechanisms in luminescent solar concentrators [12,31,32]. Simulation was restricted to excite the strip at the centre of 76 mm × 4.26 mm (front face in Fig. 1) using a 460 nm LED. The Ce:YAG LC is assumed to be a homogeneous medium and the incident photons are traced on their way through the concentrator until they reach the edges where they experience reflection, absorption, re-emission, fluorescence etc. as in Fig. 1. The photons undergo the processes in the same order as in Eq. (1). The ray tracing model is computationally expensive as a large number of rays need to be considered to obtain reasonable accuracy. Here a total of 100,000 to 200,000 rays have been considered to obtain statistically consistent results. Table 3 shows the experimental and simulation results for a single Ce:YAG strip outputting through its 4.26 mm × 0.57 mm rectangular end face and a Ce:YAG strip + optical coupler (taper) outputting through its 1.67 mm × 1.67 mm SF57 square end face, with and without a mirror attached to the non-outputting end of the Ce:YAG, respectively.

Optics EXPRESS

Table 3. Ray tracing simulation results for single Ce:YAG LC outputting light into air

	Dim. of Ce:YAG strip (mm^3)	LC	LC (end mirror)	LC with taper	LC with taper (end mirror)
Exp.	76×4.26×0.57	9.75±0.63 %	16.93±0.91 %	8.45±0.35 %	14.71±0.86 %
Sim.	76×4.26×0.57	10.5 %	19.13 %	8.59 %	14.44 %

The simulation agrees with experimental results and it was further observed that the optical efficiency can be greatly increased by adding mirrors on all sides (excluding the front and back faces, and the light outputting/butt-coupled end) of the Ce:YAG strip and optical coupler (excluding the two end faces) or using an improved coupler with no mirror needed, which could increase the efficiency by 50.15% (simulation). This is close to the calculated efficiency of 48.4% from Eq. (1) and Table 2 (with η_{trap} = 0.81). However, with our LC device comprising four Ce:YAG strips and the coupler, and with only one mirror at the end of the fourth Ce:YAG strip, we managed to get up to 20 W of CW output. A more advantageous option for upscaling the output power is to increase the lateral width of the concentrator, but here, instead, the length of the concentrator has been increased by attaching additional Ce:YAG strips of the same dimension, to the single Ce:YAG-optical coupler light source set-up. It is noticed that the trapping efficiency can be increased by aligning the fluorophores perpendicular or parallel to the waveguide surface and by optimizing the design with reflectors added to the long edges, allowing more energy emitted from the far ends [24,33]. Further, the emission from the edge where the fluorophores are aligned perpendicular to that edge is found to be ~15% higher than the isotropic case [24]. Power levels can be increased by simply scaling the pump light level and the dimensions (or illumination area) of the light source itself, which make the LC suitable in medical and other scientific applications, e.g. as a pump source for room-temperature organic masers [34]. The set-up of the room-temperature maser utilizes an organic crystal (pentacene doped p-terphenyl) that absorbs light at wavelengths which substantially overlap those emitted by Ce:YAG. Since these latest masers possess lower pump thresholds [34], we plan to pump one directly with an LC as opposed to less efficient (and more expensive) lasers. Future work encompasses an improved light source having high light extraction capability with the addition of side mirrors for optimum efficiency.

Funding

Engineering and Physical Sciences Research Council (EPSRC) grant EP/K011987/1.